Annales Geophysicae (2001) 19: 621–631

Annales Geophysicae

Dense ion clouds of 0.1 – 2 keV ions inside the CPS-region observed by Astrid-2

S. H. Høymork[1], M. Yamauchi[1], Y. Ebihara[1], Y. Narita[1], O. Norberg[1], and D. Winningham[2]

[1]Swedish Institute of Space Physics, Kiruna, Sweden
[2]Southwest Research Institute, San Antonio, USA

Received: 21 November 2000 – Revised: 12 March 2001 – Accepted: 15 March 2001

Abstract. Data from the Astrid-2 satellite taken between April and July 1999 show several examples of dense ion clouds in the 0.1–2 keV energy range inside the inner magnetosphere, both in the northern and southern hemispheres. These inner magnetospheric ion clouds are found predominantly in the early morning sector, suggesting that they could have originated from substorm-related ion injections on the night side. However, their location and density show no correlation with *Kp*, and their energy-latitude dispersion is not easily reproduced by a simple particle drift model. Therefore, these ion clouds are not necessarily caused by substorm-related ion injections. Alternative explanations for the ion clouds are the direct solar wind injections and up-welling ions from the other hemisphere. These explanations do not, however, account for all of the observations.

Key words. Magnetospheric physics (energetic particles, trapped; magnetospheric configuration and dynamics; storms and substorms)

1 Introduction

Precipitation of a few keV electrons into the auroral ionosphere has been studied by satellites for more than three decades. There are two major regions: CPS and BPS (historically acronyms for Central Plasma Sheet and Boundary Plasma Sheet, as defined by Winningham et al., 1975). The definition of CPS and BPS has since then been slightly modified (e.g. Sandahl and Lindqvist, 1990; Woch and Lundin, 1993), and we identify here the CPS as a region of unstructured trapped isotropic Maxwellian electrons with a temperature of several keV, and BPS as a region of structured electrons which are subject to some acceleration (following Newell and Meng, 1992). CPS and BPS probably correspond to diffuse and discrete aurorae, respectively. While the BPS region and discrete aurorae have been extensively studied, the CPS region, in particular its internal structure, is not so well known.

Correspondence to: M. Yamauchi
(masatoshi.yamauchi@irf.se)

We present a study of the ion clouds observed by Astrid-2 and discuss them in comparison to these three scenarios. Only ion clouds inside CPS have been considered in the present study. We do not know yet if ion clouds inside BPS (see e.g. Fig. 1) are the same as those inside CPS, and, therefore, leave it for future investigation.

The Swedish satellite Astrid-2 found several clear ion clouds in the 0.1–2 keV energy range inside CPS, i.e. on closed field lines. Ion clouds are here defined as isolated high flux ions at energies from several hundred eV to a few keV. They are not the cusp or cusp-like signatures (Sandahl et al., 1998). Figure 1 shows an example of one of the most intense ion clouds. Both (energy-latitude) dispersed and non-dispersed clouds are observed, and the observed ion clouds are denser than the ambient plasma. There are several possible sources: (1) substorm injection, (2) upward flowing ions from the conjugate hemisphere, and (3) direct magnetosheath plasma injection:

(1) Dense cold ions in the sub-keV range in the subauroral zone has been observed e.g. by Aureol (Sauvaud et al., 1981). These ions were observed in the morning sector (05–06 MLT) at invariant latitudes higher than 66°. They were found to be related to substorm-associated particle injections from the plasma sheet into the inner magnetosphere a few hours before the observation. Similar ion clouds were also found by Viking and Freja (Yamauchi et al., 1996b; Ebihara et al., 2001);

(2) Another type of sub-keV ion population inside CPS has been reported from Dynamics Explorer 1 and 2 observations (Winningham et al., 1984) and later from Aureol (Bosqued et al., 1986) and Akebono (Hirahara et al., 1997) observations. They are called "bands of ions" and show energy-latitude dispersions which are consistent with a conjugate hemisphere origin according to the convection dispersion model;

(3) Sub-keV ions with a quite different source have also been reported by Woch and Lundin (1991, 1992). Their

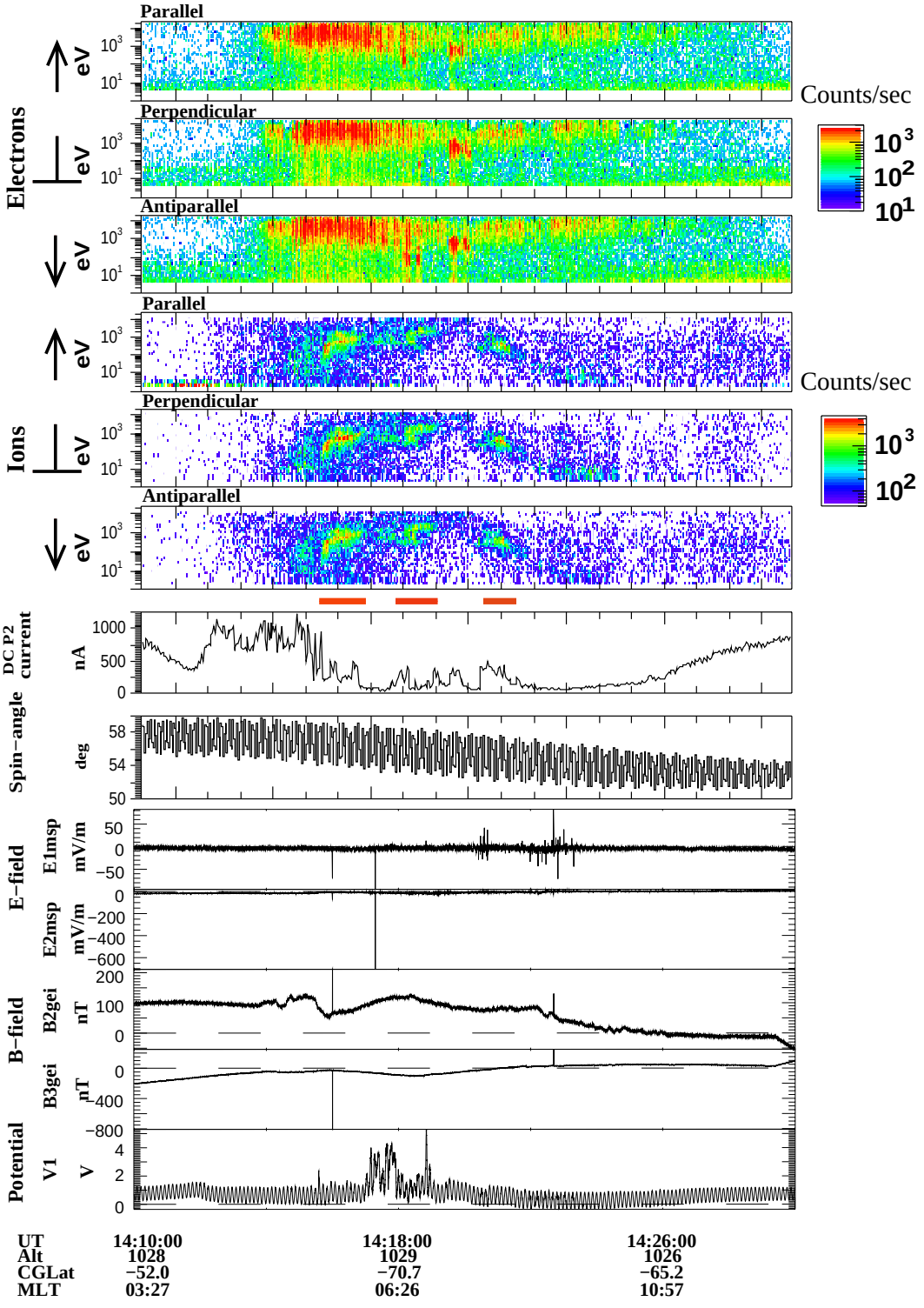

Fig. 1. Astrid-2 data for 3 July 1999 on the southern hemisphere. Distinct ion clouds (as marked by red lines) are observed. Note that only the first ion cloud is observed inside the CPS region. The other two ion clouds are not included in this study, as explained in the text. From top to bottom, three panels of data (counts/s) from the electron detectors that are most parallel (upper), most perpendicular (middle) and most anti-parallel (lower) to the geomagnetic field; three panels of data from the ion detectors (same order as for electrons); the plasma density measured as the current into the Langmuir probe; the angle between the spin-axis and the magnetic field; two panels of electric field (E1msp is the electric field component in the spin plane along the projection of model B, E2msp is the electric field component perpendicular to both E1msp and the spin axis); two panels of magnetic field (B3gei is the magnetic field component along Earth's (north) rotation axis, B2gei is the magnetic field component perpendicular to both B3gei and the direction toward vernal equinox point); and the probe potential at one of the electric field probes.

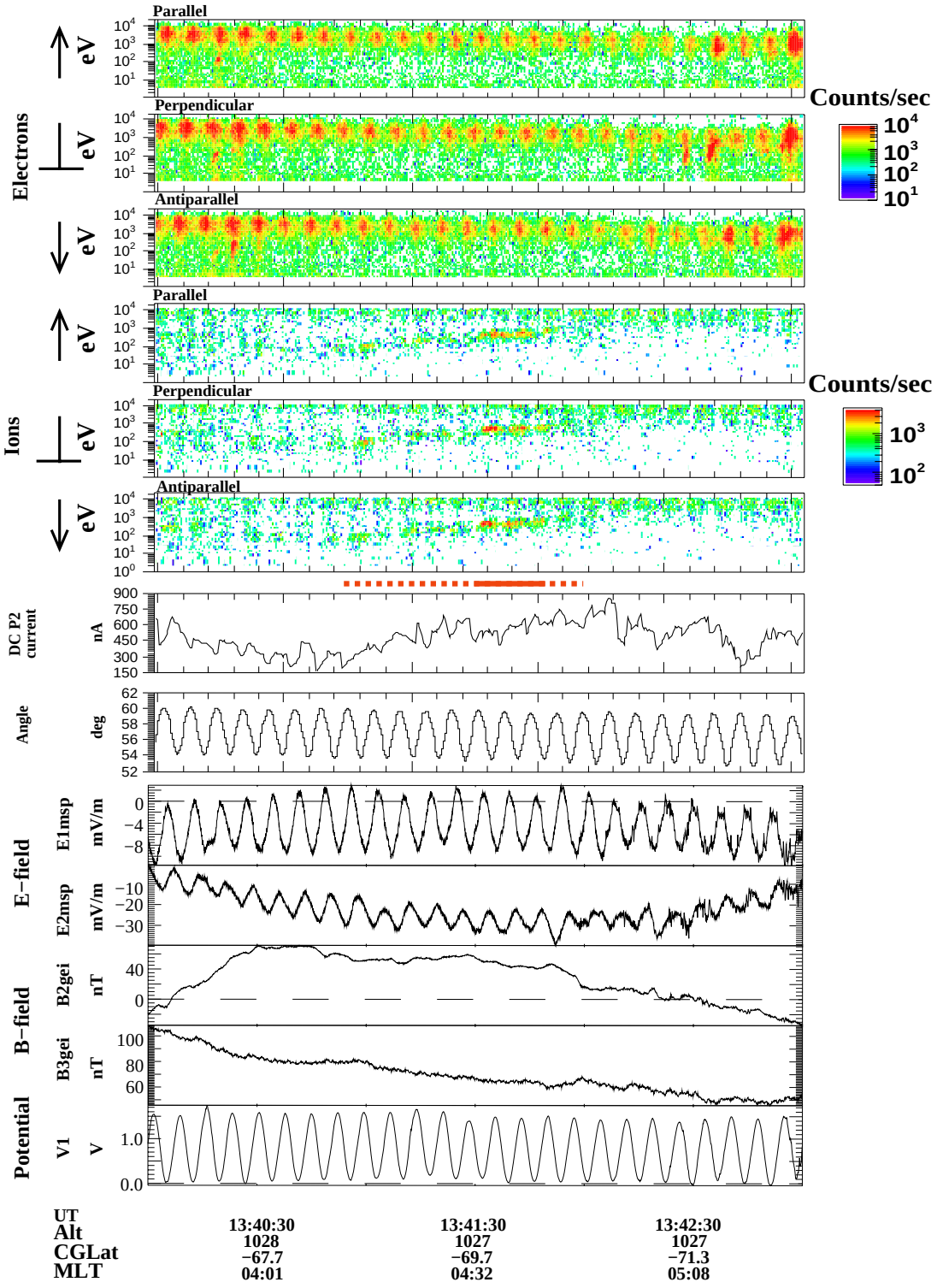

Fig. 2. Astrid-2 data for 12 July 1999 on the southern hemisphere. The data format is the same as Fig. 1. A distinct ion cloud (marked by red line) is observed inside the CPS region.

Viking data indicates that those ions, also inside the CPS region, have been directly injected from the magnetosheath. These ions are, however, temporally dispersed (decreasing energy with time) as opposed to the ion clouds observed by Astrid-2. Similar ion structures have also been observed by Interball (Sandahl et al., 1998; Sauvaud et al., 1999; Maynard et al., 2000) and by rocket (Carlson and Tobert, 1980) with a very short (steep) dispersion.

2 Instrumentation

The Astrid-2 satellite was launched in December 1998 and was operative from 11 January to 24 July 1999. Astrid-2 gathered more than 3000 traversals through the auroral region with high resolution data at 1000 km altitude. The data discussed here were taken by the MEDUSA (Miniaturized Electrostatic DUal-tophat Spherical Analyzer), LINDA (Langmuir INterferometer and Density experiment for Astrid-2) and EMMA (Electrical and Magnetic field Monitoring of the Aurora) instruments (see Marklund et al., 2001, for a more detailed description of the Astrid-2 satellite).

The MEDUSA instrument measured simultaneously ions and electrons at energies up to 18 keV/q. The particles were detected in 16 sectors in a plane almost parallel to the satellite spin plane. The temporal resolution was 8 energy sweeps/s for ions and 16 energy sweeps/s for electrons. MEDUSA was operated in two different modes, one where data from all sectors were taken (normal mode) and one where data from only three sectors were selected (select mode). We have only used data from the select mode in the present study since data from the normal mode are rare outside the auroral zone. The selected sectors were the one most parallel, the one most perpendicular and the one most antiparallel to the magnetic field. Note that the "most parallel" direction sometimes is off as much as 45° from the geomagnetic field-direction, depending on the angle between the satellite spin-axis and the magnetic field. A spin-axis perpendicular to the magnetic field gives the best pitch-angle coverage.

The plasma density was measured by the two pairs of Langmuir-probes of the LINDA instrument. The EMMA instrument measured AC and DC electric and magnetic fields. The electric fields were measured by four wire booms with spherical probes in the satellite spin plane. The magnetic fields were measured by a magnetometer mounted on an axial boom on the shadow side of the spacecraft.

3 Observations

As we defined in the introduction, ion clouds are isolated high flux ions at energies from several hundred eV to a few keV. In this paper we studied those with energy flux of more than $8{\cdot}10^{-5}$ ergs cm^{-2} st^{-1} s^{-1} eV^{-1} ($\sim 5 \cdot 10^7$ cm^{-2} st^{-1} s^{-1}). Examples of ion clouds are indicated by red lines in Figs. 1 and 2. Both (energy-latitude) dispersed and the non-dispersed ion clouds are observed; they look the same in the spectrogram except for the dispersion. The dispersed ones always show the highest energies at the highest latitudes regardless of the satellite traversal direction. We restrict our study to those inside the CPS only to make sure that they are on closed geomagnetic field lines. Note that CPS here is defined as the region of unstructured electrons (see introduction). Similar ion structures that are indistinguishable when examining only the ion data are also observed inside the BPS and on the boundary between the CPS and BPS, but we do not include them in the present study since we are not sure if they are inside the closed geomagnetic field region. The ion clouds on the open/closed boundary are naturally expected from solar wind injections. We have also omitted any ion clouds between 9 and 15 MLT to avoid direct solar wind injections which are sometimes found even inside the CPS (Yamauchi et al., 1993).

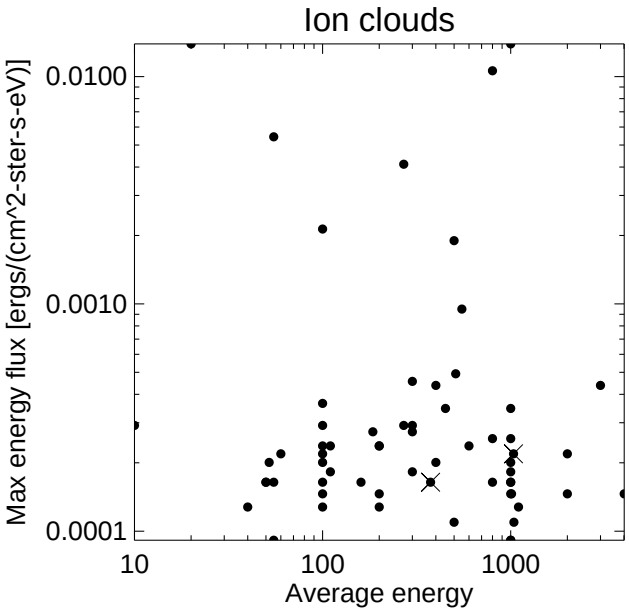

Fig. 3. Distribution of maximum energy flux and average energy of ion clouds. The chosen examples of Figs. 1 and 2 are marked by crosses.

There are three ion clouds in Fig. 1: at 14:15:20–14:16:50 UT (inside the CPS), at 14:18:00–14:19:00 (inside the BPS), and 14:20:30–14:21:20 (at the boundary between the CPS and BPS). The latter two are not included in the study, as mentioned above.

The first ion cloud in Fig. 1 shows energy-latitude dispersion. The characteristic energy increases from 40 eV at $-66°$ CGLat up to 1 keV at $-69°$ CGLat. Note that the satellite spin-axis is pointing at an angle of 50°–60° from the geomagnetic field for this period, so that the "parallel" and "antiparallel" direction in Fig. 1 is not the real field-aligned direction (off by 30–40°). The instantaneous magnetometer data shows 50–100 nT change, indicating a local field-aligned current (FAC) which is probably supported by the ion cloud. This demonstrates that the observed ion cloud is not an instrumental effect. We also note that such a current system has often been observed together with solar wind injections (Woch and Lundin, 1992), but not during substorm-related injections (Yamauchi et al., 1996a).

Figure 2 shows an example of an ion cloud that has a narrower energy range. The ion cloud is seen from 13:41:30 to 13:41:50 UT. The pitch-angle coverage is the same as for the previous one. This ion cloud is also accompanied by 100 nT magnetic field change, which corresponds to a substantial meso-scale FAC (Yamauchi et al., 1998). Such an intense

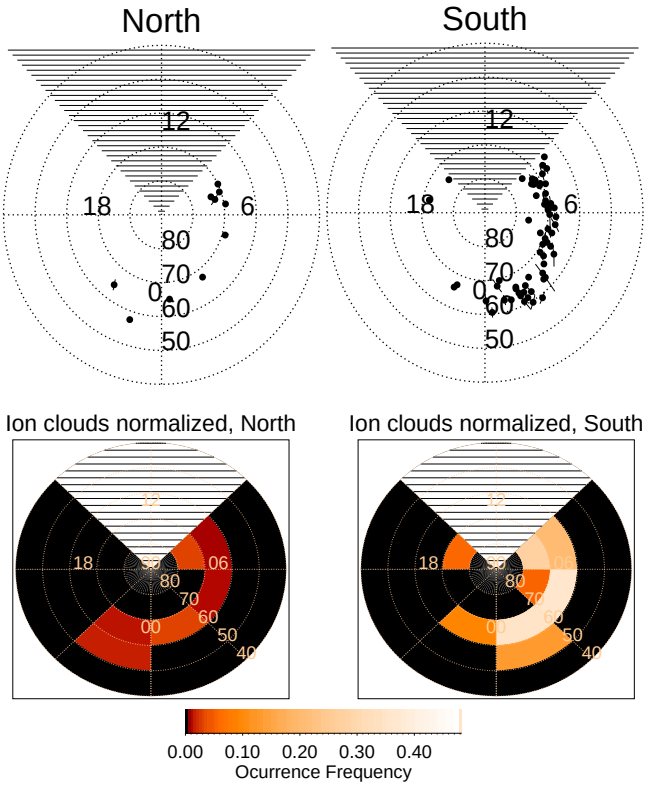

Fig. 4. Spatial distribution of ion clouds in geomagnetic coordinates in the northern (left) and southern (right) hemisphere. The upper panels show the position of individual ion clouds and the lower panels show the relative occurrence of ion clouds (number of ion clouds divided by number of satellite passes). There are, in total, 15 ion clouds observed in the northern hemisphere and 107 in the southern hemisphere. Note that ion clouds between 9 and 15 MLT are not included.

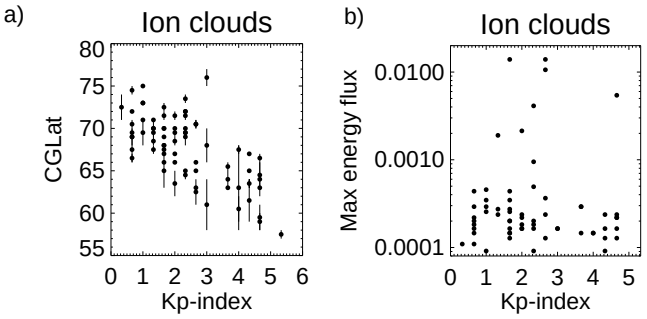

Fig. 5. **(a)** Variation in ion cloud CGLat (centers are marked by dots and extension by lines) with geomagnetic activity, *Kp*-index. **(b)** Relation between *Kp*-index and maximum flux (ergs $cm^{-2}st^{-1}s^{-1}eV^{-1}$)) in ion clouds.

FAC suggests that a net flux (upward flowing or downward flowing) exists.

We found 122 ion clouds inside the CPS from all MEDUSA particle spectra taken in April – July 1999. Figure 3 shows the distribution of maximum energy flux (we set the lower cutoff at 100 counts/s) and average energy for the observed ion clouds. This figure shows the spread in energy flux and average energy of the clouds without any obvious correlation. The two clouds in Figs. 1 and 2 are indicated by crosses in the plot; they are not extreme cases. In the following, we give a description of these ion clouds in terms of distribution, temperature, density and relation to geomagnetic activity.

Note also that we observe more ion clouds in the southern (autumn/winter) hemisphere than in the northern (spring/summer) hemisphere.

3.1 Spatial distribution

Figure 4 shows the distribution of the observed ion clouds inside the CPS in CGLat and MLT coordinates in both hemispheres. Upper panels show the distribution and lower panels show the occurrence frequency. There is a clear dawn-dusk asymmetry; more ion clouds are observed between 6–9 MLT than between 15–18 MLT in both the southern and northern hemispheres, as seen from both upper and lower panels. We note that this asymmetry is not attributed to the fact that we have restricted this study to ion clouds inside the CPS, since the same asymmetry is seen even if we include those seen inside the BPS or on the boundaries (not shown here).

3.2 Number density

We have estimated the density for four of the observed ion clouds (Figs. 1 and 2 show two of these ion clouds) by direct calculation (Paschmann et al., 1998). Table 1 shows the result of these calculations. The density of the clouds reaches 10–50 cm^{-3} and is much higher than the background density of $>$ 100 eV ions at the same location.

3.3 Geomagnetic activity dependence

Figure 5a shows the relation between the latitudinal position of ion clouds and the geomagnetic activity represented by the *Kp*-index. The correlation coefficient is found to be -0.8, indicating that the latitudinal position of ion clouds eventually moves equatorward for large *Kp*. Part of this shift is attributed to an artificial bias, since we choose ion clouds only inside the CPS. The CPS region is supposed to move equatorward when the geomagnetic activity is enhanced, as is reported by Winningham et al. (1977) using satellite particle data (see also Newell and Meng, 1994). Keeping this in mind, we can point out the following properties: the high latitude cutoff for the occurrence of clouds seems to be constant ($\sim 75°$) for *Kp* between 1– and 3. For *Kp* greater than 3, the high latitude cutoff decreases by more than 5° to a new plateau ($\sim$ 68°). The low latitude cutoff decreases linearly for all *Kp*.

Figure 5b shows the relation between the ion cloud intensity (maximum energy flux) and *Kp*, and there is no correlation between them. We should note, however, that the *Kp*-index only gives information on the geomagnetic activity av-

Table 1. Estimation of density for four of the observed ion clouds. From a direct calculation (Paschmann et al., 1998) using energies between 10 eV – 2 keV, we find the ion density of the cloud, n_{i_c}, inside the clouds and ion background density, $n_{i_{bg}}$, in the exterior. The electron background densities (n_e) inside the clouds are also from direct calculations. The maximum peak energy is also given. (Note that the background density of case 1 is uncertain, since the clouds cover almost the whole CPS in this event)

Time (UT)	Case 1[a] 03 July 1999, 14:15	Case 2[b] 12 July 1999, 13:41	Case 3 17 July 1999, 12:47	Case 4 21 July 1999, 11:22
n_{i_c} (cm^{-3})	30	10	50	50
$n_{i_{bg}}$ (cm^{-3})	< 1	~ 1[c]	< 1	~ 2[c]
n_e (cm^{-3})	1.5	1.4	2.2	3.1
Max Energy (eV)	1000	400		200

[a] Shown in Fig. 1
[b] Shown in Fig. 2
[c] Includes a CPS component at energies > 3 keV

eraged over 3 hours. Therefore, *Kp* is not a good indicator of substorms, which typically last a few tens of minutes. We have, therefore, studied four selected events in detail. They are some of the most clear cases of both dispersed and non-dispersed events (two of them are shown in Figs. 1 and 2).

Table 2 summarizes the geomagnetic conditions for these four examples of the observed ion clouds. One finds that *Kp* is low for all of the chosen cases, D_{st} varies from -30 nT (indicating minor magnetic storm) to 6 nT (quiet time), and *AE* varies from 50 nT to 250 nT. In addition, we also provide information on injection events within 6 hours prior to the observations by Astrid-2. The onset times of the injection events are estimated from the data of energetic electrons (≥ 30 keV) observed by the LANL satellite that was closest to midnight within this time interval (data not shown). The LANL satellites are in geosynchronous orbit in the equatorial plane at a geocentric distance of 6.6 Earth radii. Only one of the satellites was in the midnight MLT sector during morning UT for these four cases; this was the LANL-89, and it had a longitude of $\sim 195°$ at this time. The other four satellites were in the late morning and early afternoon sectors during noon UT. The LANL-89 data show indications of substorm injections (sudden increase in electron flux) for three of the four cases. The time (in UT) and position (in MLT) for the injections are included in Table 2. However, one of the cases, case 3 on 17 July 1999, 12:47 UT, is observed during very quiet times without any visible signature of substorm injection. The quiet condition is also verified by the provisional AE index (9 stations). Therefore, we need to consider another source mechanism, at least for those that occur during quiet times. On the other hand, the other three cases are not fully understood by substorm injection either, as is discussed below.

4 Possible mechanisms

As mentioned in the introduction, we consider three possible sources for the observed ion clouds, to be discussed in the following sub-sections.

4.1 Drifting ions from the near Earth plasma sheet

4.1.1 Possible source region

One possible scenario is that the ion cloud has drifted from the nightside plasma sheet.

To roughly investigate this hypothesis we have back-traced the observed ion clouds using the guiding center bounce-average drift velocity. For the inner magnetosphere this drift velocity is (following Ejiri, 1978; Ebihara and Ejiri, 1999) approximately given by;

$$\boldsymbol{U}_0 = \frac{\boldsymbol{E} \times \boldsymbol{B}}{B^2} + \frac{WG(\alpha_0)}{B^3} \boldsymbol{B} \times \nabla B, \quad (1)$$

The first part on the right-hand side in Eq. (1) is due to the $\boldsymbol{E} \times \boldsymbol{B}$ drift and the second part is the combined gradient $\boldsymbol{B}$ and curvature drifts. $\boldsymbol{E}$ and $\boldsymbol{B}$ are the electric and magnetic fields acting on the particles with energy W, charge q and equatorial pitch angle α_0. $G(\alpha_0)$ is given by Ejiri (1978). The Earth's geomagnetic field is assumed to be a dipole field (Lyons and Williams, 1984) and the electric field ($\boldsymbol{E} = -\nabla\Phi$) will result from a combination of the Volland-Stern type convection potential (Volland, 1973; Stern, 1975) and the corotation potential.

Figure 6 shows, as an example, the back-tracing of the ion cloud on 3 July, 14:15 UT, which is shown in Fig. 1 (also case 1 in Table 3). It takes 4.8 hours for the ion cloud to drift from the pre-midnight plasma sheet to the observation by Astrid-2. $\boldsymbol{E}$ is assumed to be constant in time during this period, corresponding to $Kp = 2- \ldots 1-$. We have calculated the estimated times when the earthward ion flow starts from the near Earth tail at pre-midnight for four of the observed ion clouds. From this we find that the possible earthward ion flow must have started from (or passed) 3.5 to 4.8 hours prior to the observations at $L = 10$ if the injection started near midnight. We also note that back-tracing shows that the azimuthal drift velocity is similar to 1 MLT/h, making it difficult for LANL-89 to miss possibly associated substorm injections.

As mentioned above, we use a dipole magnetic field model and the Volland-Stern model for the electric field. Strictly

Table 2. Overview of the geomagnetic conditions for four of the observed ion clouds: the time of observation by Astrid-2, the MLT of the observed cloud, the *Kp*, D_{st} and *AE* indexes at the observation, and time of the substorm injections, seen by LANL that occurred within 6 hours prior to the ion cloud observation by Astrid-2.

	Case 1	Case 2	Case 3	Case 4
Time (UT)	03 July 1999, 14:15	12 July 1999, 13:41	17 July 1999, 12:47	21 July 1999, 11:22
MLT (h)	5–6	4–5	3–4	3–4
Kp	1−	2	1+	2
D_{st} (nT)	−30	−23	6	−3
AE (nT)	250	200	50	250
Substorm inj. obs.	09:20 UT	10:00 UT	no substorm injection	08:10 UT
by LANL	22.2 MLT	23.0 MLT		21.1 MLT

speaking, this particle tracking should be checked with more realistic models, such as Tsyganenko's model and Weimer's model [1]. However, such an attempt is beyond the scope of this paper. We claim that the ion cloud observations are a constraint for future modeling effort.

Although the present field models are rather crude, they may be adequate for the restricted case of: 1) a small equatorial pitch-angle ($\sim 5°$), and 2) low kinetic energy (less than 10 keV at $L = 10$). Magnetic drift motion of ions with small equatorial pitch angle is governed by the curvature drift rather than the grad-B drift. At the L-shells in which we are interested, the curvature drift motion relies on the dipolar geometry. In addition, the magnetic drift contributes to the drift motion of ions for higher energies. For ions with energy less than 10 keV at $L = 10$, the $\boldsymbol{E} \times \boldsymbol{B}$ drift contributes the most to the drift motion. We believe that the Volland-Stern type convection electric field model is adequate to represent the large-scale convection electric field for a quiet period (*Kp* values used in the calculation are listed in Table 2).

4.1.2 Flux calculation

We have also profided a forward modeling of the injection for the ion cloud at 3 July 1999 (case 1 in Table 2). Figure 7 shows the simulated ion spectra along the Astrid-2 pass for three different sets of boundary conditions. According to the above back-tracing, it seems reasonable to assume that the observed 0.1 keV ions have passed $L = 10$ between 5.60 and 4.87 hours (depending on energy) before the observation. If the injection boundary is located at $L = 10$, its width is expected to extend from 22.8 to 01.0 MLT. We set this condition as the initial condition. Here, we notice that the injection is not necessarily attributed to a substorm. A long-lasting ion injection with a narrow flow channel inferred by Ebihara et al. (2001) is also possible.

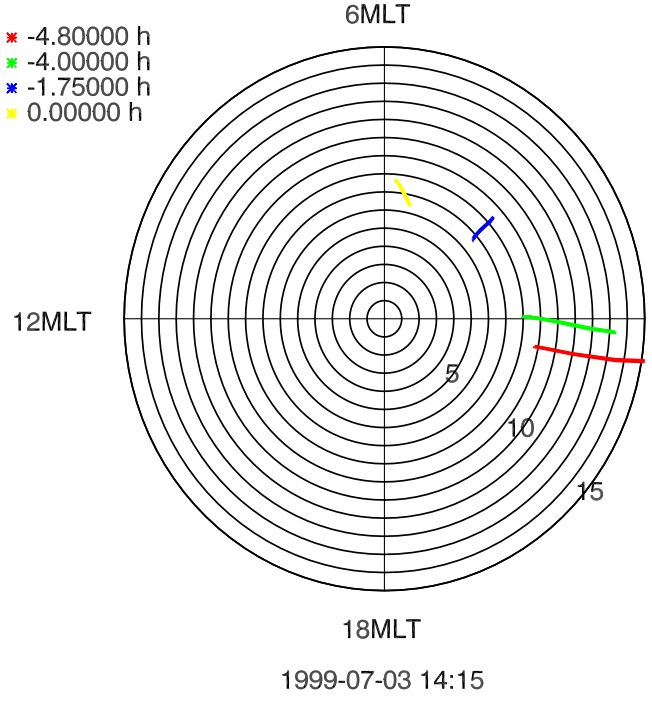

Fig. 6. Back-tracing of the ion cloud at 3 July, 14:15 UT. The exterior of the cloud is specified by energy, MLT and L-shell. The drift-velocities are given by Eq. (1). Yellow color corresponds to the measured event, while red color corresponds to the estimated time of injection (4.8 hours before).

We used 1 keV Maxwellian ions with an isotropic pitch angle distribution at the injection boundary. This choice of distribution is not critical for the simulation result. An equatorial pitch angle of 5° was chosen for the observed ion cloud in this modeling, since only ions with small equatorial pitch angles will be able to reach the satellite position (high latitude and low altitude, 1000 km), from conservation of the first adiabatic invariant.

In the first run of the simulations, we let the injection begin at 06:24:00 UT on 3 July 1999 and last until 09:37:38 UT, with the above width of the injection boundary. The simu-

[1] The Tsyganenko (Tsyganenko, 1987) model for the geomagnetic field takes into account currents in the magnetosphere and is thus usually closer to the real magnetic field than the dipole magnetic field model used here. The Volland-Stern model for the electric field could have been replaced by the Weimer's model (Weimer, 1995). This model is based on the analysis of a large number of satellite passes and is shown to be better than the Volland-Stern model during geomagnetic storms (Kistler et al., 1999).

Table 3. The time of observation by Astrid-2, the MLT of the observed cloud and the estimated flight time between Astrid-2 and assumed source region of $L = 10$.

	Case 1	Case 2	Case 3	Case 4
Time (UT)	03 July 1999, 14:15	12 July 1999, 13:41	17 July 1999, 12:47	21 July 1999, 11:22
MLT (h)	5–6	4-5	3–4	3–4
Estimated flight time (h)	4.8	4	3.5	3.5

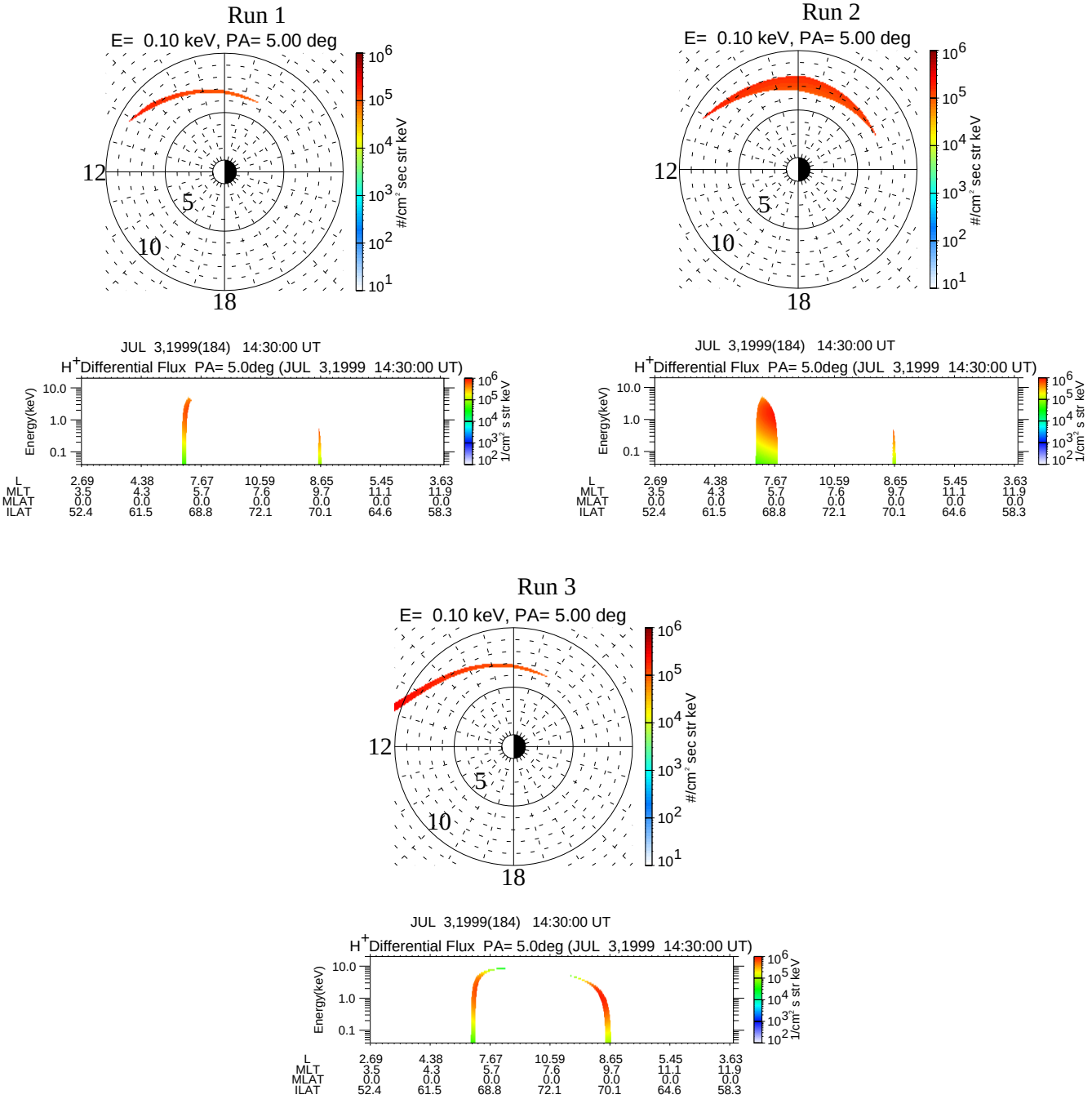

Fig. 7. Three simulations of the possible substorm injection on 3 July 1999. The three simulations are done with different boundary conditions (see description in the text). The upper panel gives the extension of the cloud at the time of observation by Astrid-2 (MLT and L-values are indicated), while the lower panel shows the resulting energy spectrum along the Astrid-2 orbit.

lated spectrum shows a disagreement with that observed by Astrid-2 (Fig. 1). The measured clear energy-latitude dispersion in Fig. 1 is not reproduced by the first run of the simulation (Fig. 7, run 1). This indicates that a more extended injection boundary or longer injection duration is needed.

In a second run, the injection duration was, therefore, extended to 06:24:00–11:36:34 UT. As seen in Fig. 7 (run 2), this extention still cannot reproduce the observed energy dispersion in the spectrum.

Next, we spread the flow channel in the near-earth tail out between 22.8 MLT and 04.0 MLT. This can produce an energy-latitude dispersion that agrees with the observation except for the upper threshold energy. The upper cutoff energy in the simulation ($\sim$ 10 keV) is much higher than that observed by Astrid-2 ($\sim$ 2 keV). Another difference is that an additional new dispersion appears for this simulation at 9 MLT in Fig. 7 (run 3). This dispersion is not seen in the Astrid-2 data.

Thus, we encounter problems in this scenario, although the dispersion pattern might be corrected by using the special $\boldsymbol{E}$-field and injection spatial distribution for the actual case (e.g. such as the one by Kistler and Larson, 2000). Such an attempt is, however, beyond the scope of this paper.

4.2 Upward parallel potential drop at conjugate hemisphere

The second possible source for the observed ion clouds is ionospheric ions accelerated upward by a parallel potential drop and associated wave activity on the other hemisphere (Winningham et al., 1984; Bosqued et al., 1986). In this case, accelerated electrons (that have been accelerated downward in the same potential) are expected on the conjugate hemisphere of the observed ion clouds. Such electrons are indeed observed by the DMSP F13 satellite, as shown in Fig. 8.

DMSP was located at the conjugate point of the ion cloud observation by Astrid-2 (same MLT and CGLat) only a few minutes earlier (14:23–14:24 UT). We see accelerated electrons in the DMSP data inside the CPS at energies comparable to the energies of the ion cloud ($\sim$ 1 keV). This indicates that a parallel potential drop probably exists above the altitude of DMSP ($\sim$ 840 km), together with some heating mechanism. Therefore, the potential drop on the conjugate hemisphere of the observed ion cloud could well be related to the ion cloud itself. However, this potential drop is probably caused by the ion cloud and not vice versa because quasi-neutrality at the equatorial plane does not mean that ions and electrons have the same mirror point (see e.g. Alfvén and Fälthammar, 1963). There are two reasons to believe so: 1) The average total number flux of upward flowing ions is typically less than $5 \cdot 10^7$ cm^{-2} s^{-1} (Øieroset et al., 1999) with densities less than 5 cm^{-3}, and that is low compared to the density inside the ion clouds (see Table 1). 2) Another problem with this scenario is the lack of correlation with *Kp*.

On the other hand, the dawn-dusk asymmetry seen in the data is consistent with the formation of parallel potential drops, since parallel electric fields from one hemisphere to the other flow predominantly from summer to winter in the dawn sector and from winter to summer in the dusk sector (Cladis and Collin, 1997). We see most of the ion clouds in the dawn sector in the winter hemisphere. One would expect an energy-pitch angle dispersion of the ions with this scenario (Winningham et al., 1984). The data discussed here does not, however, have full pitch angle coverage, so we cannot identify such a possible dispersion.

The DMSP ion data also shows a similar signature to the ion clouds discussed here. The flux of these ions is, however, below the threshold value of $8{\cdot}10^{-5}$ ergs cm^{-2}st^{-1}s^{-1}eV^{-1} $\sim 5{\cdot}10^7$ cm^{-2}st^{-1}s^{-1} chosen in this study.

4.3 Plasma from magnetosheath

The third possible mechanism of the observed ion clouds is directly injected magnetosheath ions, as reported by Woch and Lundin (1992). There are some differences between the Astrid-2 observations ($\sim$ 1000 km) and their observations by Viking ($\sim$ 10000 km). The energy dispersion of the plasma injection by Woch and Lundin (1992) was always decreasing energy in time, not in latitude (indicating a temporal injection), while the dispersions seen on Astrid-2 show energy-latitude dispersion. This difference could, however, be due to the difference in the satellite traversal velocities. Another difference is the location: the Viking observations of ion clouds are more poleward (higher than 70 CGLat) than the Astrid-2 observations (at 70 CGLat or lower, see Fig. 4) although both are inside the CPS region. More importantly, Viking observations do not have the strong dawn-dusk asymmetry, as seen in Fig. 4. The dawn-dusk asymmetry is difficult to explain by the altitude difference of the two spacecraft, while the other problem could be attributed to the altitude difference. Therefore, one also encounters problems with this scenario in explaining the ion clouds observed by Astrid-2. Note that we have not selected any ion clouds in the 9 to 15 MLT sector in order to avoid the cusp injections.

5 Discussion and conclusion

We have reported unusual and outstanding ion cloud events inside the CPS region. The ion cloud observations from Astrid-2 do not seem to agree fully with any of the above discussed possible sources:

(1) For the first scenario, a simple simulation of the ion drift from the near-Earth plasma sheet is unlikely to reproduce the observed particle energy-latitude dispersion if we use a stationary injection boundary and a simplified field model. A non-stationary injection boundary that is moving inwards with time (Reeves et al., 1996) should be included in a future simulation.

Room for future improvement also remains in the electric field and magnetic field models, although the models used herein (dipole magnetic field model and Volland-Stern electric field model) seem reasonable for the case

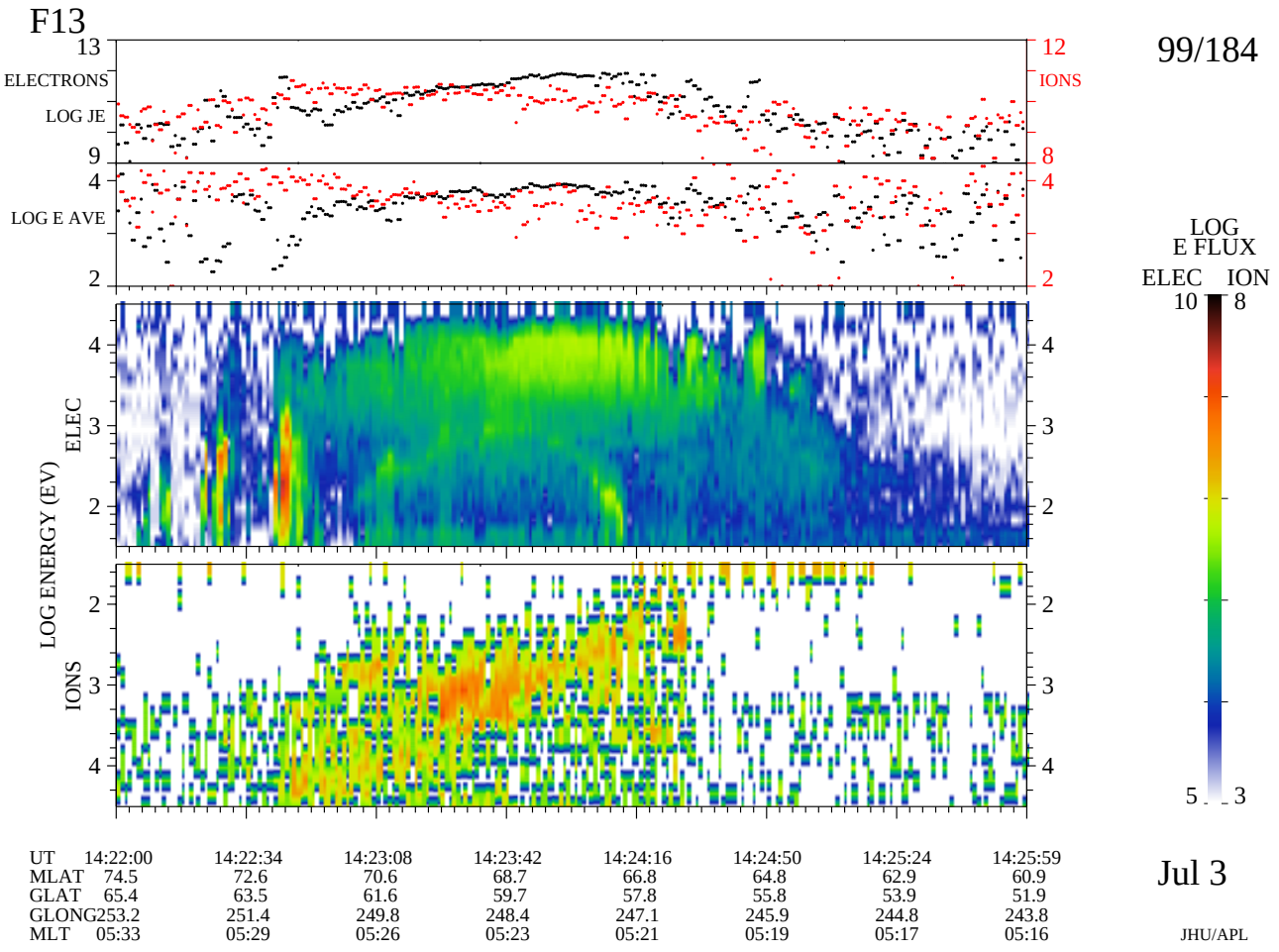

Fig. 8. DMSP F13 particle data from the conjugate point of the ion cloud observed by Astrid-2 on 3 July 1999, 14:15 (see Fig. 1). Color scale is differential energy flux in eV/(cm^2 s ster eV). (Courtesy Pat Newell)

presented (small equatorial pitch angle and low kinetic energy). A more realistic model (as discussed by e.g. Kistler and Larson, 2000) must be tested for the observed data to completely rule out the scenario of drifting ions from the near-Earth plasma sheet. It should, however, also be mentioned that one of the observed cases happens during completely quiet times (see case 3 in Table 2) and thus, must have a different explanation.

Another problem is the observed FACs which are difficult to explain by the drift model.

(2) For the second scenario, the observed ion flux is one order of magnitude higher than the expected ion flux for upward (escaping) ionospheric ions from the opposite hemisphere;

(3) For the third scenario, it is hard to explain the dawn-dusk asymmetry in the Astrid-2 observations.

Although none of the proposed scenarios accounts for all of the ion cloud observations, we cannot completely rule out any of them as the possible source of some of the observed ion clouds. The different ion clouds might have different sources.

Future investigations by multi-satellite data and more detailed simulations seem to be necessary to address the source of these ion clouds.

Acknowledgements. The Astrid-2 project is funded by the Swedish National Space Board and by corresponding agencies in the other participating countries. The *Kp*, *AE* and D_{st} indexes are obtained from WDC for geomagnetism at Kyoto University. The Astrid-2 EMMA data were provided by Lars Blomberg and Nickolay Ivchenko, and plotting software for these data by Tomas Karlsson. Astrid-2 LINDA data were provided by Bengt Holback.

The authors also thank Pat Newell for supplying us with the DMSP F13 particle data and Geoff Reeves for providing us with LANL particle data.

Topical Editor G. Chanteur thanks J. M. Grebowsky and M. Ejiri for their help in evaluating this paper.

References

Alfvén, H. and Fälthammar, C. G., Cosmical electrodynamics, fundamental principles, Clarendon Press, Oxford, 1963.

Bosqued, J. M., Sauvaud, J. A., Delcourt, D., and Kovrazhkin, R. A., Precipitation of suprathermal ionospheric ions accelerated in the conjugate hemisphere, J. Geophys. Res., 91, 7006, 1986.

Carlson, C. W. and Tobert, R. B., Solar wind ion injections in the morning auroral oval, J. Geophys. Res., 85, 2903, 1980.

Cladis, J. B. and Collin, H. L., Observations of longterm field-aligned flow of O^+ ions near the equator during summer and winter, J. Geophys. Res., 102, 22077, 1997.

Ebihara, Y. and Ejiri, M., Quantitative ring current model: overview and comparison with observations, Adv. Polar Upper Atmos. Res., 13, 1, 1999.

Ebihara, Y., Yamauchi, M., Lundin, R., and Ejiri, M., Simulation of wedge-like dispersion of sub-keV ions in the magnetosphere, J. Geophys. Res. in press, 2001.

Ejiri, M., trajectory traces of charged particles in the magnetosphere, J. Geophys. Res., 83 (A10), 4798–4810, 1978.

Hirahara, M., Yamazaki, A., Seki, K., Mukai, T., Sagawa, E., Kaya, N., and Hayakawa, H., Characteristics of downward flowing ion energy dispersions observed in the low-altitude central plasma sheet by Akebono and DMSP, J. Geophys. Res., 102, 4821, 1997.

Kistler, L. M. and Larson, D. J., Testing electric and magnetic field models of the storm-time inner magnetosphere, J. Geophys. Res., 105 (A11), 25221, 2000.

Kistler, L. M., Klecker, B., Jordanova, V. K., Möbius, E., Popecki, M. A., Patel, D., Sauvaud, J. A., Réme, H., Di Lellis, A. M., Korth, A., McCarthy, M., Cerulli, R., Bavassano Cattaneo, M. B., Eliasson, L., Carlson, C. W., Parks, G. K., Pashmann, G., Baumjohann, W., and Haerendel, G., Testing electric field models using ring current ion energy spectra from Equator-S ion composition (ESIC) instrument, Ann. Geophys., 17, 1611, 1999.

Lyons, L. R. and Williams, D. J., Quantitative aspects of magnetospheric physics, D. Reidel Publishing Company, 2nd ed., ISBN 90-277-1663-3, 1984.

Marklund, G. T., Blomberg, L. G., and Persson, S., Astrid-2, an advanced microsatellite for auroral research, Ann. Geophysicae, 19, 589–592, 2001 (this issue).

Maynard, N. C., Savin, S., Erickson, G. M., Kawano, H., Nemecek, Z., Peterson, W. K., Safranokova, J., Sandahl, I., Scudder, J. D., Siscoe, G. L., Sonnerup, B. U. Ö., Weimer, D. R., White, W. W., and Wilson, G. R., Observation of the magnetospheric "sash" and its implications relative to solar-wind/magnetospheric coupling: A multi-satellite event analysis, J. Geophys. Res., submitted, 2000.

Newell, P. T. and Meng, C.-I., Mapping the dayside ionosphere to the magnetosphere according to particle precipitation characteristics, Geophys. Res. Lett., 19 (6), 609, 1992.

Newell, P. T. and Meng, C.-I., Ionospheric projections of magnetospheric regions under low and high solar wind dynamic pressure conditions, J. Geophys. Res., 99, 273, 1994.

Øieroset, M., Yamauchi, M., Liszka, L., Christon, S. P., and Hultqvist, B., A statistical study of ion beams and conics from the dayside ionosphere during different phases of a substorm, J. Geophys. Res., 1999.

Paschmann, G., Frazakerley, A. N., and Schwartz, S. J., Eds., Analysis Methods for multi-spacecraft data, Number SR-001 in ISSI Scientific Report, International Space Science Institute, 1998.

Reeves, G. D., Henderson, M. G., McLachlan, P. S., Belian, R. D., Friedel, R. H. W., and Korth, A., Radial propagation of substorm injections, in Proc. Third international conference on substorms (ICS-3), number 389 in ESA-SP, 1996.

Sandahl, I. and Lindqvist, P.-A., Electron populations above the nightside auroral oval during magnetic quiet times, Planet. Space Sci., 38 (8), 1031, 1990.

Sandahl, I., Koskinen, H. E. J., Mälkki, A. M., Pulkkinen, T. I., Budnik, E. Y., Fedorov, A. O., Frank, L. A., and Sigwarth, J. B., Dispersive magnetosheath-like ion injections in the evening sector on January 11, 1997, Geophys. Res. Lett., 25 (14), 2569, 1998.

Sauvaud, J., Crasnier, J., Mouala, K., Kovrazhikin, R. A., and Jorjio, N., Morning sector ion precipitation following substorm injections, J. Geophys. Res., 86 (A5), 3430, 1981.

Sauvaud, J.-A., Popescu, D., Delcourt, D. C., Parks, G. K., Bittnacher, M., Sergeev, V., Kovrazhkin, R. A., Mukai, T., and Kokubun, S., Sporadic plasma sheet ion injections into the high-altitude auroral bulge: Satellite observations, J. Geophys. Res., 104, 28565, 1999.

Stern, D. P., The motion of a proton in the equatorial magnetosphere, J. Geophys. Res., 80, 595, 1975.

Tsyganenko, N. A., Global quantitative models of the geomagnetic field in the cislunar magnetosphere for different disturbance levels, Planet. Space Sci., 35, 1347, 1987.

Volland, H., A semiempirical model of large-scale magnetospheric electric fields, J. Geophys. Res., 78, 171, 1973.

Weimer, D. R., Models of high-latitude electric potentials derived with a least error fit of spherical harmonic coefficients, J. Geophys. Res., 100 (A10), 19595, 1995.

Winningham, J. et al., A statistical study of the "instantaneous" nightside auroral oval: The equatorward boundary of electron precipitation as observed by the Isis 1 satellites, J. Geophys. Res., 82, 5573, 1977.

Winningham, J. D., Yasuhara, F., Akasofu, S.-I., and Heikkila, W. J., The latitudinal morphology of 10-eV to 10-keV electron fluxes during magnetically quiet and disturbed times in the 2100-0300 MLT sector, J. Geophys. Res., 80, 3148, 1975.

Winningham, J. D., Burch, J. L., and Frahm, R. A., Bands of ions and angular V's: A conjugate manifestation of ionospheric ion acceleration, J. Geophys. Res., 89, 1749, 1984.

Woch, J. and Lundin, R., Temporal magnetosheath plasma injection observed with Viking: A case study, Ann. Geophysicae, p. 133, 1991.

Woch, J. and Lundin, R., Signatures of transient boundary layer processes observed with Viking, J. Geophys. Res., 97, 1431, 1992.

Woch, J. and Lundin, R. The low-latitude boundary layer at mid-altitudes: identification based on Viking hot plasma data, Geophys. Res. Lett., 20 (10), 979, 1993.

Yamauchi, M., Woch, J., Lundin, R., Shapshak, M., and Elphinstone, R., A new type of ion injection event observed by Viking, Geophys. Res. Lett., 20, 795, 1993.

Yamauchi, M., Lundin, R., Mursula, K., Marklund, G., and Potemra, T. A., Dayside Pc5 pulsation detected by Viking ion data at L=4, Geophys. Res. Lett., 23 (18), 2517, 1996a.

Yamauchi, M., Lundin, R., Eliasson, L., and Norberg, O., Mesoscale structures of radiation belt/ring current detected by low-energy ions, Adv. Space Res., 17, 171, 1996b.

Yamauchi, M., Lundin, R., Eliasson, L., Ohtani, S., and Clemmons, J. H., Relationship between large-, meso-, and small-scale field-aligned currents and their current carriers, in J. Moen et al., Eds., Polar cap boundary phenomena, page 173, Kluwer Academic Publishers, 1998.